Reports

Apollo 16 Far-Ultraviolet Camera/Spectrograph: Earth Observations

Abstract. *A far-ultraviolet camera/spectograph experiment was operated on the lunar surface during the Apollo 16 mission. Among the data obtained were images and spectra of the terrestrial atmosphere and geocorona in the wavelength range below 1600 angstroms. These gave the spatial distributions and relative intensities of emissions due to atomic hydrogen, atomic oxygen, molecular nitrogen, and other species—some observed spectrographically for the first time.*

One of the major objectives of the Naval Research Laboratory's far-ultraviolet camera/spectrograph, which was operated on the lunar surface during the Apollo 16 mission, was to obtain spectra and imagery of the terrestrial atmosphere and the geocorona, in the wavelength range from 500 to 1600 Å. This far-ultraviolet wavelength range contains resonance lines and bands of most of the atoms and molecules that are important in the terrestrial atmosphere and geocorona.

As an observing station, the lunar surface offers a particular advantage, relative to low earth orbit, in that it allows a comprehensive, overall view of the entire terrestrial hemisphere which faces the moon. Thus, it is possible to simultaneously observe related but widely separated phenomena, such as the polar auroras, as well as most of the hydrogen geocorona, which previous satellites and space probes have shown extends out to a distance of at least ten earth radii.

The instrument is, basically, a tripod-mounted Schmidt camera (7.5 cm aperture, $f/1.0$) that uses electronographic recording and is equipped for use either directly as a camera, or with a grating as a spectrograph. The details of the instrument and its principles of operation have already been described (*1*).

When used as a spectrograph, the instrument has two modes of operation: (i) with a LiF corrector plate, giving good spatial resolution along the spectrograph "slit" but with a short-wavelength limit at 1050 Å, and (ii) with no corrector plate, giving poorer resolution, but with a short-wavelength limit at about 500 Å set by the reflectivities of the mirror and grating coatings. This procedure also aids in separating the effects of stray light and overlapping spectral orders. The spectral resolution is about 30 Å with the corrector and 40 Å without it. The long-wavelength limit of the camera, in all modes of operation, was set by the KBr photocathode response at about 1600 Å.

In the direct imaging mode it is also possible to separate the contributions of the various species, to some extent, by the use of selective filtering. In the present case, it was possible to separate the effects of atomic hydrogen, which has a resonance line at 1216 Å (the Lyman-α line), from those of atomic oxygen and molecular nitrogen, which have resonance transitions longward of 1250 Å, by taking photographs with two different corrector plates on the Schmidt camera: (i) a LiF corrector plate, which cuts off at 1050 Å, and (ii) a CaF_2 corrector plate, with a short-wavelength limit at 1250 Å.

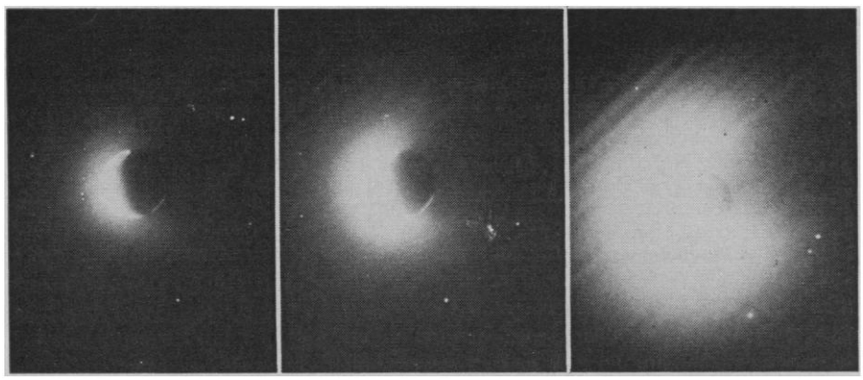

Fig. 1. The earth photographed in the wavelength range from 1050 to 1600 Å, with exposure times of about 5, 15, and 60 seconds, showing the hydrogen geocorona, day airglow, and polar auroras. The diagonal streaks in the longer exposures are instrumental.

Figure 1 shows the earth as photographed in the wavelength range from 1050 to 1600 Å, with exposure times of about 5, 15, and 60 seconds. The diffuse emission due to the hydrogen geocorona is quite apparent, and the general appearance is similar to that inferred from the lower-resolution photometry of earlier experiments. Of particular new interest in these photographs, however, are fine structural details, such as those of the shadow boundary. The fact that the dark limb of the earth is seen silhouetted against the far-side geocoronal radiation is of considerable interest for interpretations of radiative transfer.

Also evident in Fig. 1 are the polar auroral zones, in which the radiation is largely due to atomic oxygen and molecular nitrogen, rather than atomic hydrogen. The ultraviolet day airglow is much less intense, relative to the aurora, than the reflected and scattered light in the visible wavelength range. Therefore, the aurora is readily seen on the day, as well as the night, side of the earth in the 5-second exposure. Almost the entire northern auroral ring is visible, but only a portion of the southern auroral zone, most of which is on the far side of the earth. Exposures made with the CaF_2 corrector, which excludes the Lyman-α line of hydrogen, are shown in Fig. 2. These exposures were of much longer duration; therefore, the auroras in these pictures are greatly overexposed and structural details are obliterated.

The ultraviolet day airglow shows a strong limb-brightening effect, since it is the result of emission from a relatively thin layer. It is due mostly to excitation by energetic photoelectrons, produced from air molecules by extreme-ultraviolet and x-ray photons from the sun. (The Lyman-α glow, however, is mainly due to resonance scattering of the solar Lyman-α emission by geocoronal hydrogen atoms.)

Figure 2 shows images of the earth

obtained with exposures of 3, 10, and 30 minutes in the wavelength range from 1250 to 1600 Å. The day airglow of atomic oxygen and molecular nitrogen is visible in Fig. 2. Since the scale heights of these species are much less than that of atomic hydrogen, the edge of the sunlit earth is much sharper in this wavelength range, and only a relatively small additional extent is revealed with longer exposure times.

Of particular interest in the longer exposures at 1250 to 1600 Å are two airglow bands at low magnetic latitudes on the dark side of the earth. Night airglow zones occurring at plus and minus 15° on either side of the magnetic dip equator had previously been observed in the far-ultraviolet from the OGO-IV (orbiting geophysical observatory) satellite (*2, 3*). However, at least the southernmost of the two bands seen in Fig. 2 has a significant curvature and turns northward at a significant angle to the magnetic equator, appearing to approach and cross the other band.

Figure 3 is a diagram of the earth as seen from the Apollo 16 site at the time the photographs in Fig. 2 were taken. It appears that, at the terminator, the airglow bands start out symmetrically opposite the magnetic dip equator. They then close in and cross it, and each other, near the antisolar meridian. The 30-minute exposure also reveals a general dark-side airglow, which is evident by its sharp cutoff at the edge of the dark-side disk.

Figure 4 shows spectra of the earth taken during the Apollo 16 mission. In these exposures, the spectrograph slit crossed the earth at approximately a 34° angle to the sun line.

Figure 4A, a 10-minute exposure with the LiF corrector, reveals the resonance lines of atomic oxygen at 1304 and 1356 Å, as well as the hydrogen Lyman-α line at 1216 Å. The oxygen emissions are seen to be mostly confined to the sunlit disk of the earth, terminating sharply at the sunlit limb, whereas the Lyman-α radiation is much more pervasive, showing only a relatively mild concentration toward the sunlit disk. (There is, in fact, a component of the Lyman-α radiation from interplanetary space, which is seen in all directions from the lunar surface.) The dark limb of the earth is also evident in the Lyman-α line, as a step increase in intensity as the far side of the geocorona starts to contribute to the observed radiation. A similar step increase is also observed at the sunlit limb in a shorter (3-minute) exposure. Hence, the disk of the earth in pure Lyman-α radiation appears dark in projection against the far-side geocorona, on the sunlit as well as the night side.

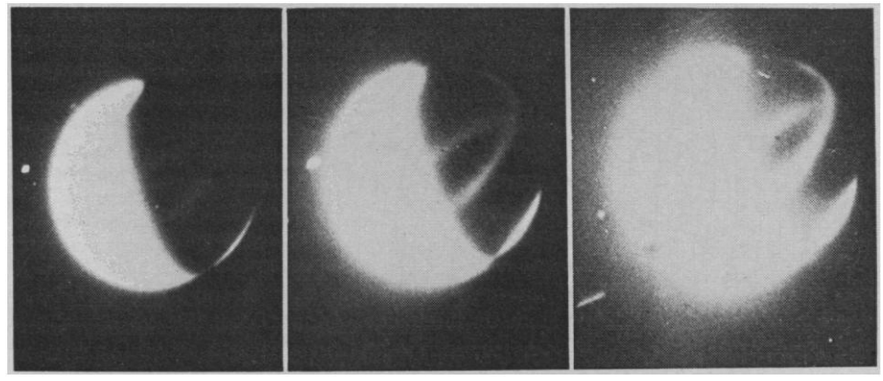

Fig. 2. The earth photographed in the wavelength range from 1250 to 1600 Å, with exposure times of 3, 10, and 30 minutes. This wavelength range excludes radiations of the hydrogen geocorona, but includes those of atomic oxygen and molecular nitrogen in the upper atmosphere.

Figure 4B, a 30-minute exposure with the LiF corrector, reveals emissions in the Lyman-Birge-Hopfield bands of N_2 longward of the oxygen resonance lines.

Figure 4C, a 130-minute exposure with the LiF corrector, also shows features shortward of Lyman-α, which are attributed to the Birge-Hopfield bands of N_2, and resonance lines of N, O, and possibly N^+ (see table 1).

Figure 4D, a 30-minute exposure with no corrector plate, reveals the resonance line of He at 584 Å, the resonance line of O^+ at 834 Å, and the

Table 1. Tentative spectral identifications. The numbers in the first column correspond to the numbers in Fig. 4, C and D. Wavelengths are designated by λ.

Number	Measured λ (Å)	Tentative identification		
		Species	Transition	λ (Å)
1	584*	He	$2p\ ^1P^o \rightarrow 1s^2\ ^1S$	584.3
2	740	(?) Ne	$3s[1\frac{1}{2}]^o \rightarrow 2p^6\ ^1S$	743.7
			$3s'[\frac{1}{2}]^o \rightarrow 2p^6\ ^1S$	735.9
3	835	O^+	$2p^4\ ^4P \rightarrow 2p^3\ ^4S^o$	834.5
				833.3
				832.8
4	990	N_2	$b\ ^1\Pi_u \rightarrow X\ ^1\Sigma_g^+$ (0, 0)	985.7
			(0, 1)	1008.6
		O	$3s'\ ^3D^o \rightarrow 2p^4\ ^3P$	988.8
				990.2
				990.8
5	1030	H	$3p\ ^2P^o \rightarrow 1s\ ^2S$	1025.7
		O	$3d\ ^3D^o \rightarrow 2p^4\ ^3P$	1025.8
				1027.4
				1028.2
		N_2	$b\ ^1\Pi_u \rightarrow X\ ^1\Sigma_g^+$ (0, 2)	1032.6
6	1085	N_2	$b\ ^1\Pi_u \rightarrow X\ ^1\Sigma_g^+$ (0, 4)	1083.1
		N^+	$2p^3\ ^3D^o \rightarrow 2p^2\ ^3P$	1085.7
				1084.6
				1084.0
				1085.5
				1084.6
7	1135	N	$2p^4\ ^4P \rightarrow 2p^3\ ^4S^o$	1135.0
				1134.4
				1134.2
8	1150	O	$3s^1\ ^1D^o \rightarrow 2p^4\ ^1D$	1152.1
9	1216*	H	$2p\ ^2P^o \rightarrow 1s\ ^2S$	1216.7
10	1305	O	$3s\ ^3S^o \rightarrow 2p^1\ ^3P$	1302.2
				1304.9
				1306.0
11	1355	O	$3s\ ^6S^o \rightarrow 2p^4\ ^3P$	1355.6
				1358.5
		N_2	$a\ ^1\Pi_g \rightarrow X\ ^1\Sigma_g^+$ (6, 2)	1353.0
			(3, 0)	1353.7
12	1500	N	$3s^2\ ^2P \rightarrow 2p^3\ ^2D^o$	1492.6
				1494.7
		N_2	$a\ ^1\Pi_g \rightarrow X\ ^1\Sigma_g^+$ (3, 3)	1493.2
			(0, 1)	1506.8
			(4, 4)	1508.1

* By comparison with laboratory spectra taken with the instrument during preflight calibrations.

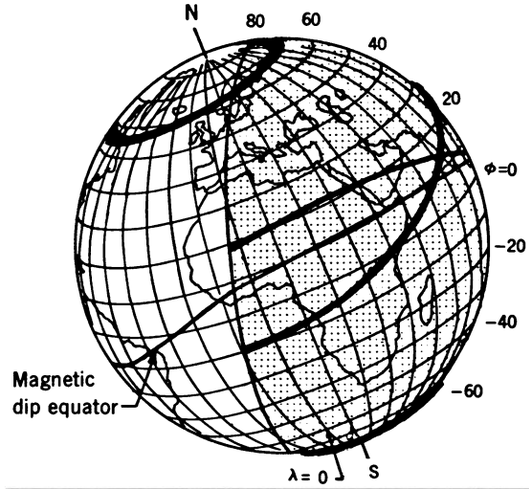

Fig. 3. A diagram of the earth as seen from the Apollo 16 landing site at the time of the far-ultraviolet observations. The approximate locations of the magnetic dip equator and the observed tropical night airglow bands and polar auroras are indicated. λ, Longitude; φ, latitude.

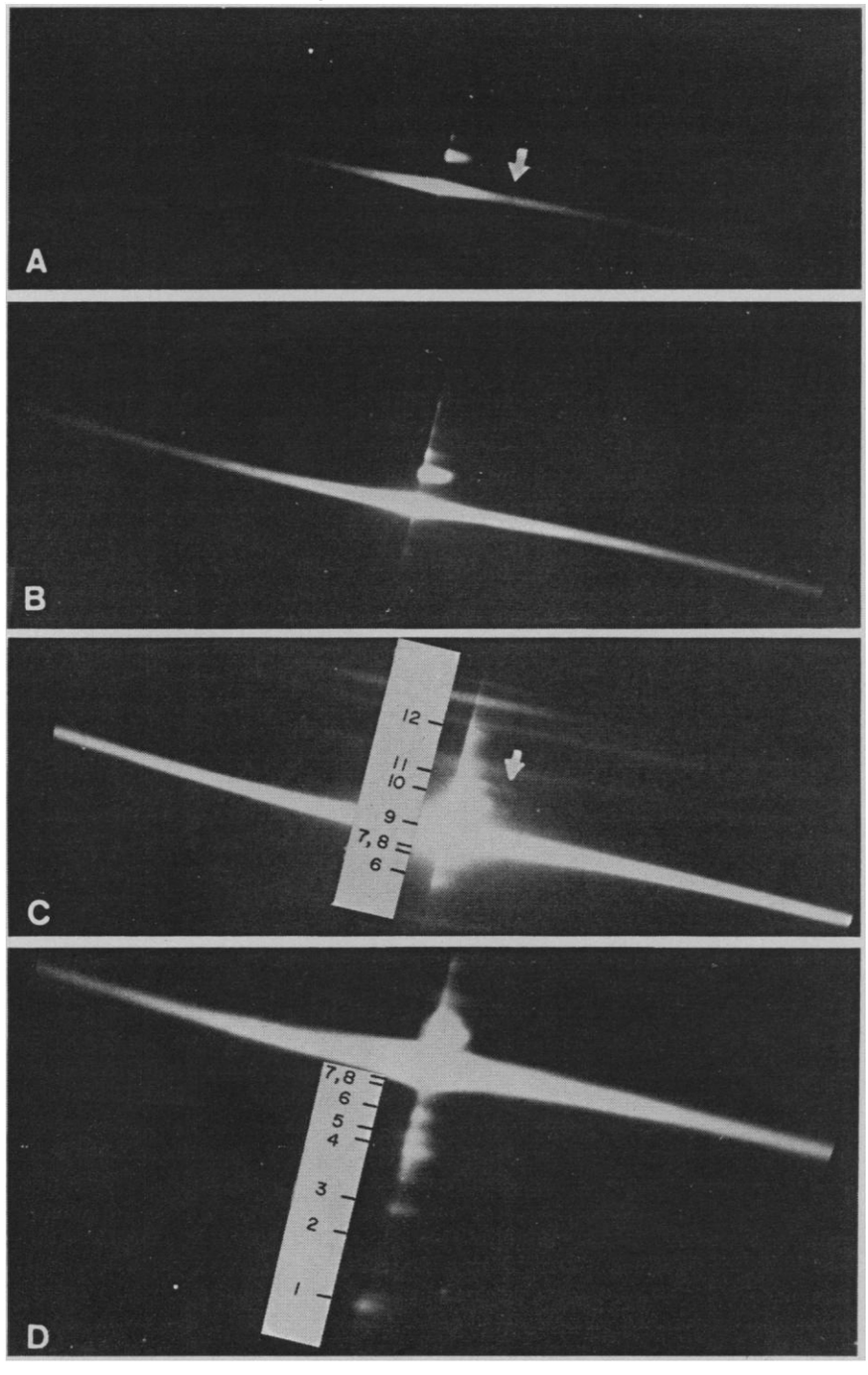

Fig. 4. Far-ultraviolet spectra of the earth taken during the Apollo 16 mission. (A) A 10-minute exposure, with LiF corrector, revealing atomic oxygen emissions (terminating sharply at the sunlit limb) and the atomic hydrogen Lyman-α line (extending across the field). The dark limb of the earth, as revealed in the Lyman-α line, is indicated by an arrow. (B) A 30-minute exposure with LiF corrector, revealing additional features due to molecular nitrogen. (C) A 130-minute exposure with LiF corrector. Features tentatively identified in Table 1 are numbered. The arrow indicates atomic oxygen emissions in the night-side tropical airglow belts. (D) A 30-minute exposure with no corrector plate, extending the spectral coverage down to below 500 Å, and revealing emissions of helium and ionized oxygen (see Table 1). Unmarked "lines" extending across the field are instrumental.

Lyman-β resonance line of hydrogen at 1026 Å, as well as strong blended emissions longward of about 900 Å, which are probably mostly due to the Birge-Hopfield and other permitted resonance band systems of N_2. Recombination of O^+ into the ground state of O may also contribute near 910 Å (*4*). The Lyman-β line at 1026 Å is readily identified separately from the other transitions which can contribute at this wavelength because, like the Lyman-α line, it has a very large emission scale height. The scale height of the He emission at 584 Å, as expected, is intermediate between those of the hydrogen lines and the oxygen and nitrogen transitions. A faint feature near 740 Å may be due to the resonance transition of Ne; however, the positive detection of Ne is hindered by a deep minimum of the KBr photocathode quantum yield in this wavelength region, as well as the relatively low expected abundance of Ne.

We believe that these spectra represent the first firm spectrographic identifications of the He, O^+, and H Lyman-β transitions in the terrestrial airglow. It appears that feature 6, near 1085 Å, must be at least in part attributed to the N^+ resonance line, which has also not been reported previously. Although the (0,4) Birge-Hopfield band of N_2 falls at 1083.1 Å, the (0,3) band at 1057.4 Å would be expected to be nearly as strong as the (0,4) transition, which is not the case in these spectra. The lines of O and N at 1152 and 1134 Å, respectively, are overlapped, but nevertheless distinguishable, in the 130-minute exposure with the LiF corrector. Although both fall within the nominal range of previous experiments, neither seems to have been previously

reported. The resonance line of N at 1200 Å is blended with the far more intense Lyman-α line in our spectra and is not distinguishable therein.

Figure 4C also reveals the spectrum of the dark-side airglow bands, which are evident only in the oxygen resonance lines. In agreement with the OGO-IV spectrometric results of Barth and Schaffner (*3*), the ratio of the intensity at 1356 Å to that at 1304 Å is nearly unity in the equatorial night airglow, whereas it is much less than unity in the day airglow. The mechanism responsible for the equatorial airglow is still highly controversial, in that it must account not only for the abnormal intensity ratio of the oxygen lines but also for the lack of any other emissions (such as the Lyman-Birge-Hopfield bands of N_2) and for the localization in zones near the magnetic equator. The two mechanisms that seem to be the prime contenders are (i) O^+ recombination, by the processes

$$O^+ + e \rightarrow O(^5S, {}^3S) \quad (4) \quad (1)$$

$$O^+ + O^- \rightarrow O(^5S, {}^3S) + O \quad (5) \quad (2)$$

followed by radiative de-excitation to the ground (^3P) state of O, and (ii) excitation of O atoms by low-energy (about 10 ev) electrons, which would excite $O(^5S)$ to a larger extent, relative to the $O(^3S)$ and N_2 excited states, than the higher-energy auroral electrons or day-side photoelectrons (*2*). At present, the recombination mechanism seems most likely (*6*), although the phenomenon still cannot be regarded as well understood.

The results presented here have been necessarily preliminary and qualitative, as the detailed analysis of the images and spectra will require several months.

GEORGE R. CARRUTHERS
THORNTON PAGE
E. O. Hulburt Center for Space Research, Naval Research Laboratory, Washington, D.C. 20390

References and Notes

1. R. Hillenbrand, *Sky Telesc.* **43**, 153 (1972); T. Page, *Mercury* **1**, 4 (1972); H. J. P. Arnold, *Brit. J. Photogr.* **119**, 310 (1972).
2. G. T. Hicks and T. A. Chubb, *J. Geophys. Res.* **75**, 6233 (1970).
3. C. A. Barth and S. Schaffner, *ibid.*, p. 4299.
4. W. B. Hanson, *ibid.* **74**, 3720 (1969); *ibid.* **75**, 4343 (1970).
5. W. C. Knudsen, *ibid.*, p. 3862; R. E. Olson, J. R. Peterson, J. Moseley, *ibid.* **76**, 2516 (1971).
6. E. C. Zipf and E. J. Stone, *ibid.*, p. 6865.
7. We thank our co-workers at the Naval Research Laboratory and the National Aeronautics and Space Administration; the several subcontractors who contributed to the camera preparation and to the success of the mission; and astronaut John Young, who operated the equipment on the lunar surface. Supported by a NASA grant for the Apollo 16 S201 experiment.

14 June 1972

Body Temperature of Dermochelys coriacea: Warm Turtle from Cold Water

Abstract. *The deep body temperature of a leatherback turtle,* Dermochelys coriacea, *taken out of cold water, was 18°C above the water temperature. A large size favoring heat retention from muscular activity is probably responsible for this differential. Cooling rates* (k) *in water, measured on a second animal, were in the order of 0.001°C per minute per degree of difference between body and ambient temperature.*

Leatherback turtles, *Dermochelys coriacea*, appear quite often along the coast of Canada and New England, especially at the end of the summer (*1*), yet they do not nest north of Florida. These northern appearances may reflect a regular migration, associated with feeding on jellyfish, rather than occasional stray animals (*1*). If this is so, it becomes of interest to know how these reptiles manage thermally in water of about 12°C (*1, 2*), some 15°C, below that at their nesting beaches (*3*). There are speculations that leatherbacks might be endothermic (*4*), and Mrosovsky and Pritchard (*3*) have predicted that leatherbacks could be 10° to 15°C above ambient temperatures in cold water. Unfortunately, due to their infrequent capture and poor survival in captivity and to the difficulty in handling such massive animals, opportunities for taking measurements on live specimens from cold water are very limited. We report here the first temperature data on leatherbacks kept in cold water; these indicate that this reptile is adapted to maintain its body temperature in northern seas as well as in the tropics.

The first animal studied, a male weighing 417 kg (920 pounds), with a straight-line carapace length of 156 cm, was entangled in a fishing net off Seaforth, Nova Scotia on 26 July 1971 and tethered in a tidal pool until the next day. On 27 July, it was transported to the Fisheries Research Board of Canada Laboratory at Halifax and placed in an indoor tank (3 by 3.7 m, water 1.1 m deep) for the next 24 hours. During this time fresh seawater from the bottom of the harbor was pumped through the aquarium at about 350 liter/min. The temperature of the tank containing the turtle was 7.5°C as measured by a telethermometer (Yellow Springs Instrument model 42 SC). The temperature of the input, monitored continuously (Honeywell Servoline recorder) for several years, virtually never varies more than 1.0°C in 24 hours, and runs 0.5° to 1.0°C cooler than the tank with the turtle. While it was in the tank the animal swam vigorously for long periods at about 40 strokes per minute, raising its head for breathing about two or three times per minute.

The turtle was lifted from the tank in a cargo net at 1600 hours on 28 July, placed plastron down on a cart, and then moved 100 m along a wharf, from which it was immediately transferred onto a wooden shipdeck. The animal lay on its carapace without struggling. From 1700 hours until its liberation at 1820 hours, the turtle was hosed several times with surface seawater (about 17°C) and kept covered with wet burlap. During the time the animal was outdoors before its release there was mild sunshine and some haze; air temperature was about 26°C.

Starting at 1615 hours, temperatures were taken to the nearest 0.25°C with a model 42 SC telethermometer, which was calibrated against ice water during the measurement period. The deep body temperature when first measured was 18°C above the water temperature of the tank from which the turtle had been taken (Table 1).

To assess the significance of this large temperature differential in these circumstances it is necessary to know something about how fast leatherback turtles can cool and warm. For this information we turn to data obtained on a second animal, in which it was possible to monitor temperatures of the animal while it was being cooled.

The second leatherback, a female weighing 134 kg (295 pounds), with a carapace length of 124 cm, was caught in a net on 17 October 1971, about 40 miles northwest of Key West, Florida. After being placed in an outdoor pool the turtle damaged its anterior flippers. From 19 October onward it was harnessed by a nylon net with a line running from the middorsal region to above the center of the pool; this prevented further impact with the walls but left the turtle free to make swimming movements. A blood sample was taken on 20 October. At 1030 hours on 23 October, the turtle with